Limiting and overlimiting conductance in field-effect gated nanopores

Yang Liu,[1,a)] David E. Huber,[2] and Robert W. Dutton[1]
[1]*Center for Integrated Systems, Stanford University, Stanford, California 94305, USA*
[2]*Genome Technology Center, Stanford University, Palo Alto, California 94304, USA*

(Received 2 April 2010; accepted 25 May 2010; published online 23 June 2010)

Numerical modeling of the coupled ionic and fluidic transport in field-effect gated nanopores reveals highly nonlinear current-voltage characteristics, including cross-over, rectification, and particularly limiting and overlimiting conductance. The limiting and overlimiting characteristics are shown to be greatly enhanced by the inherently coupled fluid flow and correlate with electrokinetic phenomena such as concentration polarization and vortex formation. The underlying reason for the observed nonlinear characteristics is explained by considering the symmetry properties of the electrical biasing. © *2010 American Institute of Physics*. [doi:10.1063/1.3457350]

Nanofluidic devices based on nanochannels or nanopores have been extensively studied for active control of ionic[1–8] and molecular[1,9,10] transport. The basic principle that underlies the active transport control is the modulation of the channel electrostatics via field effects, either by modifying surface charges at the channel walls[2,5] or by electrically biasing the potential at adjacent gate electrodes.[1,3,4,6–10] In such devices, the ionic transport, fluidic transport, and channel electrostatics are inherently coupled, resulting in highly nonlinear current-voltage characteristics.[6] Among the nonlinear characteristics, current rectification has been extensively explored.[6,11] This letter will focus on another important nonlinearity, the limiting and overlimiting conductance, a phenomenon where the ionic current saturates under moderate driving biases but overcomes this saturation and rises rapidly under high biases.[12] Although commonly observed in permselective nanochannels accompanying electrokinetic phenomena such as concentration polarization (CP), fluidic vortex formation and dynamic instability,[12–15] this conductance nonlinearity has not been investigated in detail in active nanofluidic devices. In this letter, we numerically model nonlinear transport within an electrically gated nanopore device and demonstrate gate-controlled limiting and overlimiting conductance. We also examine the correlation of the nonlinear conductance with CP and vortex formation, and reveal their physical origin by considering the symmetry properties of the electrical biasing.

Our model device consists of a 300 nm thick solid-state membrane with a cylindrically symmetric, 50 nm radius pore bridging two electrolyte reservoirs. A schematic showing the device with its embedded gate electrode is given in Fig. 1(a). The drain bias (V_d), applied between the drain and grounded source electrodes in the reservoirs, drives the transport processes. The gate bias (V_g), applied at the buried gate electrode, modulates the channel electrostatics via field effects.

We model the nanopore transport by self-consistently solving the coupled Poisson–Nernst–Planck (PNP) and Stokes equations under steady state conditions. Specifically, the ionic transport is governed by the continuum-based PNP equations as follows:

$$\nabla \cdot (\varepsilon_w \nabla \psi) + q(C_+ - C_-) = 0,$$

$$q\nabla \cdot (-D_+ \nabla C_+ - \mu_+ C_+ \nabla \psi + C_+ \vec{u}) = 0,$$

$$-q\nabla \cdot (-D_- \nabla C_- + \mu_- C_- \nabla \psi + C_- \vec{u}) = 0,$$

where ψ is the electrostatic potential, q the elementary charge, $C_\pm$ the cation/anion concentrations, ε_w the solution permittivity, $\mu_\pm$ the cation/anion mobilities, $D_\pm$ the cation/anion diffusion coefficients, and $\vec{u}$ the solvent velocity. The bulk salt concentration, C_0, is approached at the top and bot-

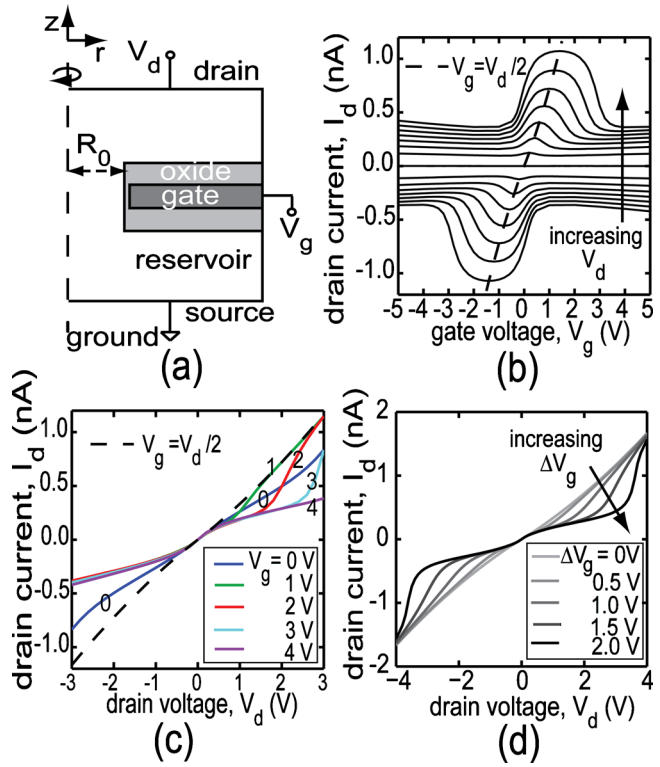

FIG. 1. (Color online) (a) Schematic of a gated nanopore device with cylindrical symmetry (not to scale). Some device parameters include: pore radius R_0=50 nm; top and bottom oxide thickness 100 nm each; gate electrode thickness 100 nm; side-wall gate oxide thickness 2 nm; reservoir size 1 μm in both width and thickness; (b) I_d vs V_g characteristics for constant V_d values that range from −2.8 to 2.8 V at a step of 0.4 V. The dashed curve corresponds to the current at symmetric bias conditions, $I_d(V_d=2V_g, V_g)$; (c) I_d vs V_d characteristics for constant V_g values that range from 0 to 4 V at a step of 1 V. The specific V_g values are labeled at each curve. The dashed curve again corresponds to the current at symmetric bias conditions, $I_d(V_d, V_g=V_d/2)$; and (d) I_d vs V_d characteristics for constant ΔV_g values that range from 0 to 2 V at a step of 0.5 V.

a)Electronic mail: yangliu@gloworm.stanford.edu.

tom boundaries. Within the oxide regions, the electrostatics is governed by the Poisson equation. The fluid transport is modeled as an incompressible, Newtonian Stokes flow and governed by the Stokes-divergence equations, including the electrical body force term and ionic osmotic pressure

$$-\nabla p + \gamma \Delta \vec{u} - q(C_+ - C_-)\nabla \psi - k_B T \nabla (C_+ + C_-) = 0,$$

$$\nabla \cdot \vec{u} = 0,$$

where p is the solvent pressure, γ the solvent viscosity, k_B the Boltzmann constant, and $T=300$ K the room temperature. The model details including the boundary conditions are described elsewhere.[8] For a given set of electrical biases V_d and V_g, the transport equations are solved to give the steady-state, terminal I-V characteristics, $I_d(V_d, V_g)$.

Some physical parameters used in this study include the following: $\varepsilon_w = 80\varepsilon_0$ for water where ε_0 is the vacuum permittivity; symmetric ion mobilities $\mu_+ = \mu_- = 7.62 \times 10^{-8}$ $m^2/V\,s$ for KCl; $\varepsilon_{ox} = 3.9\varepsilon_0$ for SiO_2; and $\gamma_0 = 0.001$ Ns/m^2 for water. The Einstein relation, $D = \mu k_B T/q$, is used. The bulk electrolyte concentration C_0 is 1 mM, corresponding to a Debye length Λ_D of 10 nm. We model a charge-neutral nanopore surface to highlight the role of electrical gating. The presence of surface charges leads to additional gating that complicates the transport but the limiting and overlimiting conductance is generally observed in our simulations.

The major subject of this work is the drain current versus drain bias (I_d-V_d) characteristics, as shown in Fig. 1(c). To understand the strong nonlinearity in I_d-V_d's, we first examine the drain current versus gate bias (I_d-V_g) characteristics and note that I_d-V_d and I_d-V_g plots are just different representations of the same device characteristics. Hence, their nonlinearities share the same physical origin. In Fig. 1(b), the simulated I_d-V_g curves exhibit a fourfold symmetry, $I_d(V_d, V_g) = I_d(V_d, V_d - V_g)$ and $I_d(V_d, V_g) = -I_d(-V_d, -V_g)$, as expected from the symmetries in device structure and in ion mobilities. Despite the fact that the pore radius is considerably larger than Λ_D ($R_0 \approx 5\Lambda_D$), significant gate modulation is observed. In a previous work, we analyzed this extended gating effect and attributed it to the descreening of the gating potential by strong ion transport.[8] Here, emphasis is given to the fact that the current is the greatest when the gate modulation is minimum, i.e., under symmetric biasing ($V_g = V_d/2$). As V_d shifts away from symmetric biasing, gate modulation significantly suppresses the current, as shown in Fig. 1(b).

By examining the I_d-V_d curves in Fig. 1(c), three features are of primary interest. First, the curves cross over each other at positive V_d's. Second, rectification is observed, where low and high conductance states are asymptotically approached at negative and positive V_d's, respectively. Third and most intriguingly, limiting conductance occurs at moderately positive V_d's, and overlimiting conductance at highly positive V_d's. Before analyzing these nonlinear features further in the following sections, it is worth noting that similar nonlinearities have recently been experimentally observed in the current-voltage characteristics of gated, conical-shape nanopores.[6]

The cross-over occurs at $V_d = V_{g1} + V_{g2}$ for any two curves with gate biases of V_{g1} and V_{g2}, respectively. This is a direct manifestation of the symmetry properties observed in Fig. 1(b). The rectification in I_d-V_d's is also explained by examining the I_d-V_g's in Fig. 1(b), where the symmetry line of current peaks is at an angle to the vertical axis. For a specific positive V_g (e.g., $V_g = 2$ V), the current approaches the symmetry line at more positive V_d's and reaches the high conductance regime. In contrast, the current moves away from the symmetry line and becomes suppressed at more negative V_d's. This asymmetry in the electrical biasing therefore leads to the rectification behavior.

More insight can be obtained by replotting the I_d-V_d's for constant ΔV_g's in Fig. 1(d), as compared to those for constant V_g's in Fig. 1(c). The transformation, $\Delta V_g = V_g - V_d/2$, counts the amount of gate potential from the symmetric bias condition. In this transformed representation, the characteristics of limiting and overlimiting conductance are more clearly observed. The I_d-V_d curve with minimum gating ($\Delta V_g = 0$) is asymptotically approached by those with more significant gating ($\Delta V_g > 0$) at both negative and positive V_d's. Furthermore, both the cross-over and rectification are absent in this constant ΔV_g representation. This strongly indicates that they intrinsically associate with the limiting and overlimiting conductance and are essentially a manifestation of the symmetry properties of the electrical biasing in the constant V_g representation.

To understand the limiting and overlimiting behavior, we study a specific I_d-V_d curve with a constant ΔV_g of 1.5 V in Fig. 2(a). For comparison, two more curves are simulated by artificially increasing the solvent viscosity to $2\gamma_0$ and $10\gamma_0$, while keeping the ion mobility unchanged. The nonlinearity is significantly reduced at higher viscosities, revealing the crucial role of the coupled fluid transport. In the following, four bias conditions are examined specifically for different V_d values, 0.1 V (A), 1.5 V (B), 3 V (C), and 4 V (D), for the case of nominal viscosity. The four conditions represent different conductance regimes as follows: linear (A), limiting (B), and overlimiting (C and D).

The key understanding of the limiting and overlimiting conductance is obtained by inspecting the normalized electrostatic potential, ψ/V_d, along the nanopore's longitudinal axis for the four bias conditions, as shown in Fig. 2(b). The effect of gate potential ($\Delta V_g = 1.5$ V) is to raise the potential inside the nanopore. This effect is the least significant in the case of low V_d (case A), which is expected because the transport is near equilibrium and the gate potential is strongly screened by counter-ions. The insignificant gate modulation is consistent with the linear I_d-V_d characteristics in this regime. As V_d increases, the counter-ion screening becomes suppressed due to enhanced transport, leading to a gate modulation of channel electrostatics far beyond Λ_D.[8,16] As a result, we observe a highly asymmetric potential profile in case B, where potential drop predominantly occurs at one side of the channel. In this regime, the current is limited by the strong gate modulation. As V_d increases further so that $V_d/2 \geq \Delta V_g$, the gate potential continues to be less screened but cannot exceed its maximum limit, ΔV_g. Consequently, the *relative impact* of the gate modulation on the overall channel electrostatics becomes smaller, as shown by the reduced asymmetry in the normalized potential (cases C and D). In this regime, the symmetric biasing condition is reached in the limit as V_d approaches infinity. The ionic conductance therefore asymptotically approaches that under the symmetric biasing, thus exhibiting the overlimiting behavior.

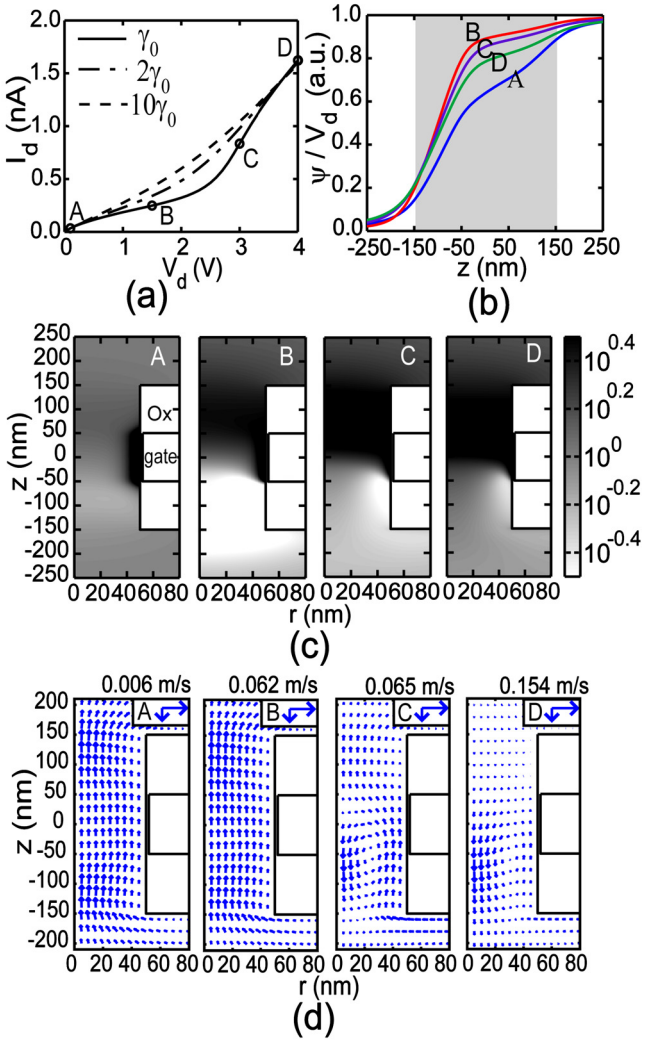

FIG. 2. (Color online) (a) Simulated I_d-V_d curve for a constant ΔV_g of 1.5 V. Four specific bias points are marked for different V_d biases, 0.1 V (A), 1.5 V (B), 3.0 V (C), and 4.0 V (D), respectively. The two broken curves are from additional simulations with higher viscosities, $2\gamma_0$ and $10\gamma_0$; (b) normalized electrostatic potential (ψ/V_d) along the nanopore longitudinal axis for the four bias points, where the shaded region indicates the channel portion; (c) profiles of the normalized ion concentration, $\bar{C}=(C_+ + C_-)/2C_0$, for the four bias points, where the gray scale corresponds to logarithmic magnitude; and (d) vector plots of fluid velocity distribution for the four bias points, where the velocity scale references are given for both radial and vertical directions in each subfigure.

CP is also observed as a result of the electrical gating. In Fig. 2(c), the normalized total ion concentration, $\bar{C}=(C_+ + C_-)/2C_0$, is shown in a logarithmic scale for the four bias conditions. In general, the ions deplete and accumulate at the bottom and top portions of the channel, respectively. The magnitude of CP is found to strongly correlate with the potential profiles in Fig. 2(b). The CP is insignificant in case A and becomes very strong in case B. It then gradually reduces as the overlimiting regime is reached in cases C and D. Such a correlation is expected: the ion concentration is low in the high-field region and vice versa to maintain ionic flux continuity.

The fluid transport is examined in Fig. 2(d), where the solvent velocity fields are shown for the four bias conditions. Induced electro-osmotic flow along the vertical direction is observed with an increasing magnitude from case A to case B. As the overlimiting regime is reached in case C, vortex formation is observed in the ion depletion zone at the bottom. The vortex flow is further enhanced in case D, and this trend continues as the symmetric biasing condition is asymptotically approached at higher V_d's.

As noted above, the association of vortex formation and overlimiting conductance has been experimentally observed in perm-selective nanochannels.[14,15] Rubinstein *et al.*[13] proposed that the convective mixing by vortices reduces CP and causes the overlimiting conductance. However, that explanation does not apply to the gated nanopore device in this study. The impact of coupled fluid transport observed in this work is to suppress the current in the limiting regime rather than to raise it in the overlimiting regime. This is evident in Fig. 2(a), where the conductance difference due to viscosity change is actually smaller in the overlimiting regime than in the limiting regime. Further confirmation follows from inspection of the relative difference in ion concentration due to viscosity change from $10\gamma_0$ to γ_0.[17] It is observed that the relative difference is reduced to below 15% in the overlimiting regime (case D), as compared to ~45% in the limiting regime (case B). We therefore conclude that, although their appearances are associated, the vortex formation is not the dominant cause of the overlimiting conductance in the gated nanopore device.

In summary, modeling of the coupled ionic and fluidic transport in field-effect gated nanopore devices reveals gate-controlled, strongly nonlinear current-voltage characteristics, including cross-over, rectification, and limiting and overlimiting conductance. Correlations with electrokinetic processes such as CP and vortex formation have been demonstrated, and the crucial role of the inherently coupled fluid transport has been identified. The physical origin of these nonlinear characteristics has been explained by considering the symmetry properties of the electrical biasing. In particular, the limiting conductance results from asymmetric biasing, when the gating effect is significant, and the overlimiting conductance from more symmetric biasing, when the relative impact of the gating effect becomes smaller due to the dominance of the applied drain bias.

[1]R. Karnik, R. Fan, M. Yue, D. Li, P. Yang, and A. Majumdar, Nano Lett. **5**, 943 (2005).
[2]H. Daiguji, Y. Oka, and K. Shirono, Nano Lett. **5**, 2274 (2005).
[3]M. Gracheva, D. Melnikov, and J. Leburton, ACS Nano **2**, 2349 (2008).
[4]R. Fan, S. Huh, R. Yan, J. Arnold, and P. Yang, Nature Mater. **7**, 303 (2008).
[5]E. Kalman, I. Vlassiouk, and Z. Siwy, Adv. Mater. (Weinheim, Ger.) **20**, 293 (2008).
[6]E. Kalman, O. Sudre, I. Vlassiouk, and Z. Siwy, Anal. Bioanal. Chem. **394**, 413 (2009).
[7]S. Nam, M. Rooks, K.-B. Kim, and S. Rossnagel, Nano Lett. **9**, 2044 (2009).
[8]Y. Liu, D. Huber, V. Tabard-Cossa, and R. Dutton, arXiv:1005.5187v2 (unpublished).
[9]K. Chun, S. Mafe, P. Ramirez, and P. Stroeve, Chem. Phys. Lett. **418**, 561 (2006).
[10]M. Taniguchi, M. Tsutsui, K. Yokota, and T. Kawai, Appl. Phys. Lett. **95**, 123701 (2009).
[11]Z. S. Siwy, Adv. Funct. Mater. **16**, 735 (2006).
[12]A. Höltzel and U. Tallarek, J. Sep. Sci. **30**, 1398 (2007).
[13]I. Rubinstein and B. Zaltzman, Phys. Rev. E **62**, 2238 (2000).
[14]S. Kim, Y.-C. Wang, J. Lee, H. Jang, and J. Han, Phys. Rev. Lett. **99**, 044501 (2007).
[15]H.-C. Chang and G. Yossifon, Biomicrofluidics **3**, 012001 (2009).
[16]Y. Liu, J. Sauer, and R. Dutton, J. Appl. Phys. **103**, 084701 (2008).
[17]See supplementary material at http://dx.doi.org/10.1063/1.3457350 for ion concentration difference due to viscosity change.